substance: Nd_2S_3
property: crystal structure, physical properties

α-Nd_2S_3

crystal structure orthorhombic (D_{2h}^{16} – Pnma)

lattice parameters

a	7.42 Å	limit of stability < 900°C;	71B
b	15.95 Å	color black; thermal conductivity	
c	4.22 Å	data [73S]	
a	7.442(2) Å		68S
b	15.519(3) Å		
c	4.029(2) Å		

electrical conductivity

σ	35 Ω^{-1} cm^{-1}	68S

β-Nd_2S_3

crystal structure tetragonal (D_{4h}^{20} – $I4_1/acd$)

lattice parameters

a	14.99 Å	limit of stability 900...1300°C;	71B
c	19.90 Å	thermal conductivity [73S]	

γ-Nd_2S_3

crystal structure cubic (Th_3P_4-defect structure, T_d^6 – $I\bar{4}3d$)

lattice parameters

a	8.527 Å	60P, 81K
	8.533(1) Å	82N
	8.522 Å	85Z

melting point

T_m	2010°C	60P, 72G
	1860°C	81K

density

d	5.50(1) g cm^{-3}	82N

energy gap and other energy parameters

E_g	2.50 ± 0.1 eV	optical gap	85Z
	2.4 ± 0.25 eV	thermodynamic	85Z
	1.9 eV	X-ray spectra	83S
	3 eV	optical absorption	70H
	2.5 eV	optical absorption	80S

E_b	5.6 eV	S 3p-level	MgKα XPS, Fig. 14 (E_b rel. to E_F)	91K
	5.6 eV	Nd 4f-level	MgKα XPS, Fig. 14	
	14.5 eV	S 3s-level	MgKα XPS, Fig. 14	
	20.6 eV	Nd $5p_{3/2}$-level	MgKα XPS, Fig. 14	
	24.3 eV	Nd $5p_{1/2}$-level	MgKα XPS, Fig. 14	
	41 eV	Nd 5s-level	MgKα XPS, Fig. 14	
	121 eV	Nd $4d_{5/2}$-level	MgKα XPS, Fig. 15	
	123 eV	Nd $4d_{3/2}$-level	MgKα XPS, Fig. 15	
	983 eV	Nd $3d_{5/2}$-level	AlKα XPS, Fig. 16	
	1005 eV	Nd $3d_{3/2}$-level	AlKα XPS, Fig. 16	
E	6.3 eV	S 3p-E_F	ELS, Fig. 17	91K
	12.1 eV	S 3p-cond. band, surface plasmon	ELS, Fig. 17	
	16.7 eV	bulk plasmon	ELS, Fig. 17	
	22.5 eV	Nd 5p-E_F	ELS, Fig. 17	
	30.6 eV	Nd 5p-5d	ELS, Fig. 17	
	≈ 44 eV	Nd 5s-E_F	ELS, Fig. 17	
	135 eV	Nd 4d-4f	ELS, Fig. 18	

phonon wavenumbers

$(\nu/c)_{TO}$	192 cm^{-1}			79A
	235 cm^{-1}			
	243.9 cm^{-1}		IR measurements	80S
	270.2 cm^{-1}			
	298.5 cm^{-1}			
$(\nu/c)_{LO}$	305 cm^{-1}			79A
	250.9 cm^{-1}			80S
	292.3 cm^{-1}			
	338.4 cm^{-1}			

dielectric constants

$\varepsilon(0)$	13			80S
	18.35			79A
$\varepsilon(\infty)$	7.0			80S
	7.1			79A, 79Z

activation energy

E_A	2.7...3.8 meV		electrical measurement	77T

electrical conductivity

σ	10^{-10} Ω^{-1} cm^{-1}	n-type		70H, 80S
	10^{2} Ω^{-1} cm^{-1}	S-excess		70H
	$1...2 \cdot 10^{-3}$ Ω^{-1} cm^{-1}			74T

Further figures and references:

coordination polyhedra: Fig. 1

heat capacity: Fig. 4

thermal conductivity: Fig. 5 and [73S]

anomaly of temperature dependent **thermal expansion coefficient**: Fig. 6

Raman spectra: Fig. 7

absorption and transmission spectra: Figs. 8, 9, 10; see also Fig. 2

reflectivity spectrum: Fig. 3

temperature dependence of **electrical conductivity**: Fig. 11

temperature dependence of **thermoelectric power** and **Hall coefficient**: Figs. 12, 13

References:

60P Picon, M., Domange, L., Flahaut, J., Guittard, M., Patrie, M.: Bull. Soc. Chim. Fr. 2 (1960) 221.
66H Holtzberg, F., Methfessel, S.: J. Appl. Phys. 37 (1966) 1433.
68S Sleight, A. W., Prewitt, C. T.: Inorg. Chem. 7 (1968) 2282.
70H Henderson, J. R. Muramato, M., Gruber, J. B., Menzel, R.: J. Chem. Phys. 52 (1970) 2311.
71B Besancon, P.: Doctor Thesis, Univ. René Descartes, Paris 1971.
72G Goryachev, Yu. M., Kutsenok, T. G.: High Temp. High Press. 4 (1972) 663.
72S Smirnov, I. A.: Phys. Status Solidi (a) 14 (1972) 363.
73S Smirnov, I. A., Parfeneva, L. S., Sergeeva, V. M., Zhukova, T. B.: Sov. Phys. Solid State 14 (1973) 2142.
74T Taher, S. M. A., Gruber, J. B., Olsen, L. C.: J. Chem. Phys. 69 (1974) 2050.
77T Taher, M. A., Gruber, J. B.: Phys. Rev. B 16 (1977) 1624.
79A Arkatova, T. G., Zhuze, V. P., Karin, M. G., Kamarzin, A. A., Kukharskii, A. A., Mikhailov, B. A., Shelykh, A. I.: Sov. Phys. Solid State 21 (1979) 1979.
79Z Zhuze, V. P., Kamarzin, A. A., Karin, M. G., Sidorin, K. K., Shelykh, A. I.: Sov, Phys. Solid State 21 (1979) 1968.
80S Skornyakov, G. P., Ponosov, Y. S., Surov, M. E., Darienko, E. P., Kamarzin, A. A., Sokolov, V. V.: Sov. Phys. Solid State 22 (1980) 613.
81K Kamarzin, A. A., Mironov, K. E., Sokolov, V. V., Malovitskii, Y. N., Vasil'yeva, I. G.: J. Cryst. Growth 52 (1981) 619.
82N Nabutovskaya, O. A., Nogteva, V. V., Sokolov, V. V., Kamarzin, A. A.: Sov. Phys. Solid State 24 (1982) 834.
83S Soldatov, A.V., Gusatinskii, A.N., Karin, M.G., Sidorin, K.K., Sadovskaya, O.A.: Inorg. Mater. 19 (1983) 951-954.
85Z Zhuze, V.P., Karin, M.G., Sidorin, K.K., Sokolov, V.V., Shelykh, A.I.: Sov. Phys. Solid State 27(12) (1985) 2205.
91K Kaciulis, S., Latisenka, A., Plesanovas A.: Surf. Sci. 251/252 (1991) 330.

Fig. 1.

Th_3P_4-type compounds. The coordination polyhedra of the cations and the anions. Full circles: Th- atoms, other circles: P-atoms [66H].

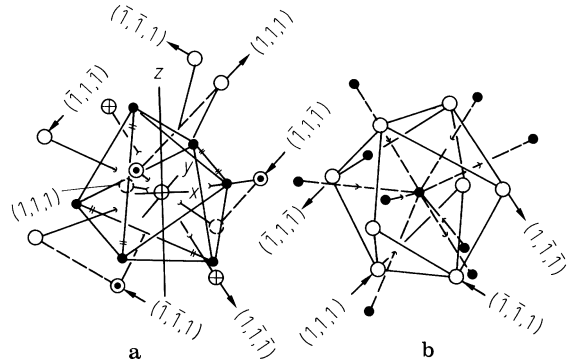

Fig. 2.

γ-La_2S_3, γ-Nd_2S_3, γ-Dy_2S_3. Absorption coefficient vs. photon energy [79Z].

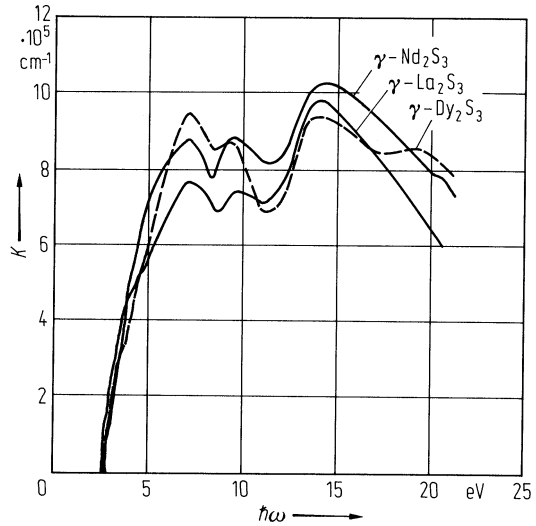

Fig. 3.

γ-La_2S_3, γ-Nd_2S_3, γ-Dy_2S_3. Reflectivity vs. wavenumber in the infrared range [79A].

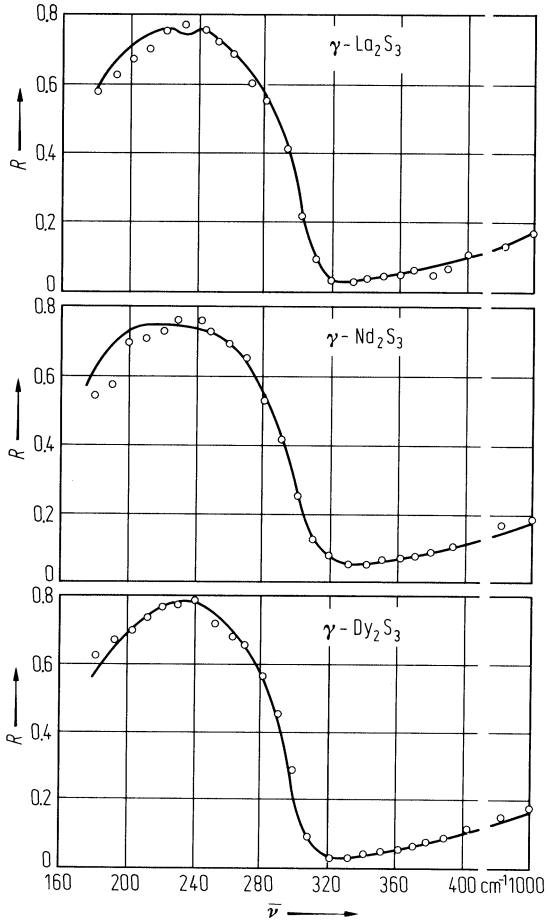

Fig. 4.

γ-Nd_2S_3, Nd_2Se_3, Nd_2Te_3. Molar heat capacity vs. temperature [72S].

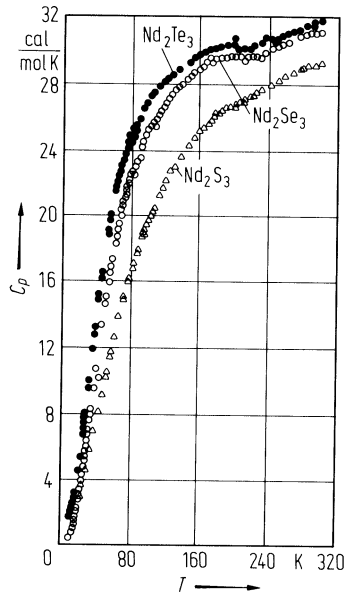

Fig. 5.

γ-Nd_2S_3, γ-Gd_2S_3, γ-Dy_2S_3. Thermal conductivity vs. temperature of several single crystals. The samples show the following excess metal content: Nd_2S_3 (*1*): 0.7% Nd, Nd_2S_3 (*2*): 0.6% Nd, Gd_2S_3 (*1*): 0.4% Gd, Gd_2S_3 (*2*): 0.5% Gd, Dy_2S_3 (*1*): 0.1% Dy, Dy_2S_3 (*2*): 0.2% Dy [77T].

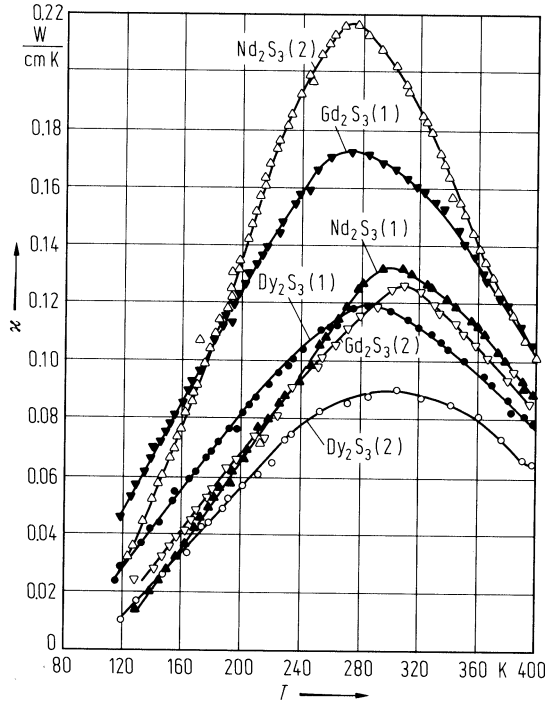

Fig. 6.

γ-Nd_2S_3. Linear thermal expansion coefficient vs. temperature showing an anomaly. (*1*): values obtained after preliminary cooling below 169 K, (*2*): values obtained when the sample was not cooled below 169 K [82N].

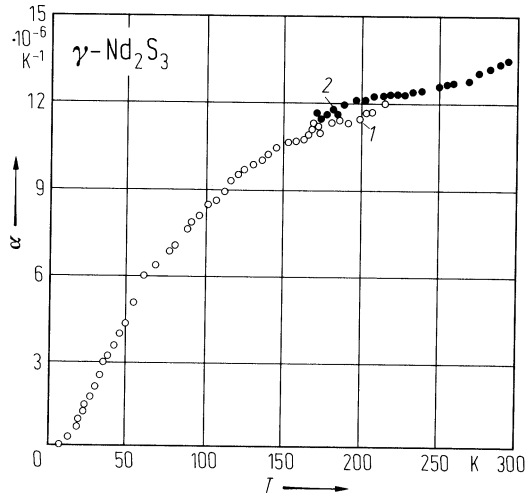

Fig. 7.

γ-Nd_2S_3. Raman spectra (intensity vs. Raman shift) in the Stokes (a) and anti-Stokes (b) regions for different polarizations [80S].

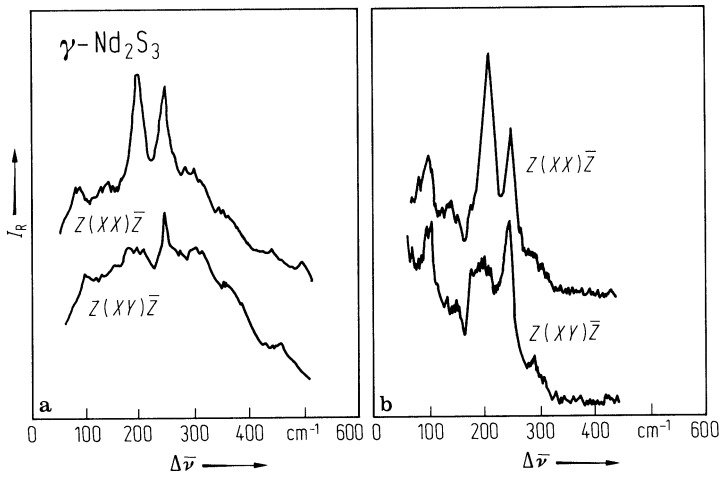

Fig. 8.

γ-Nd_2S_3. Absorption coefficient vs. wavelength at 80 K, uv-region, Nd^{3+}-ground state multiplets are indicated [70H].

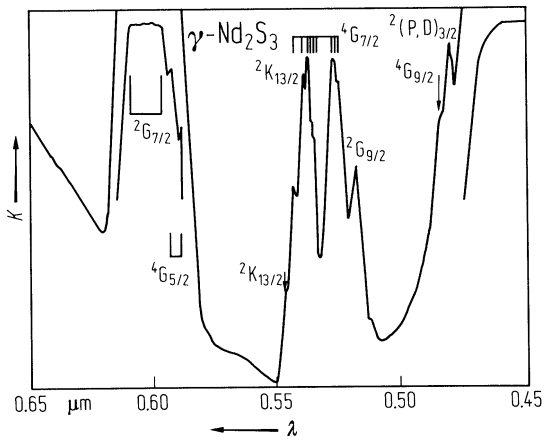

Fig. 9.

γ-Nd_2S_3. Absorption coefficient vs. wavelength at 80K, ir-region, Nd^{3+}-ground state multiplets are indicated [70H].

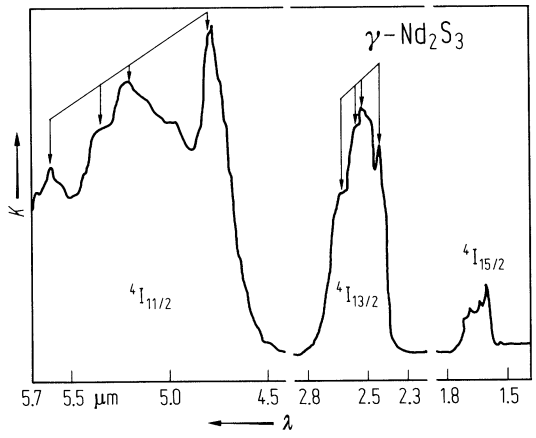

Fig. 10.

γ-Nd_2S_3. Transmission vs. wavelength of a 0.07 mm thick crystal [80S].

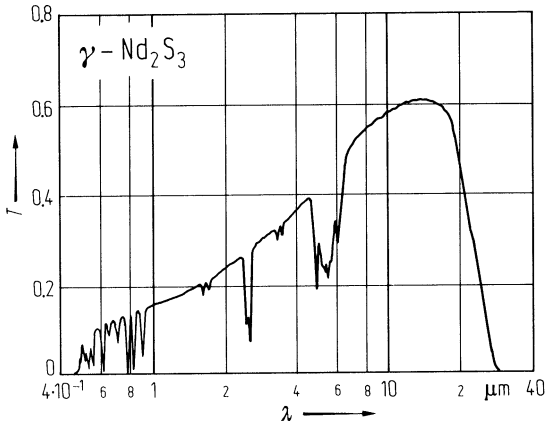

Fig. 11.

γ-Nd_2S_3, γ-Gd_2S_3, γ-Dy_2S_3. Temperature dependence of the electrical conductivity. The sample compositions are given in Fig. 5 [77T].

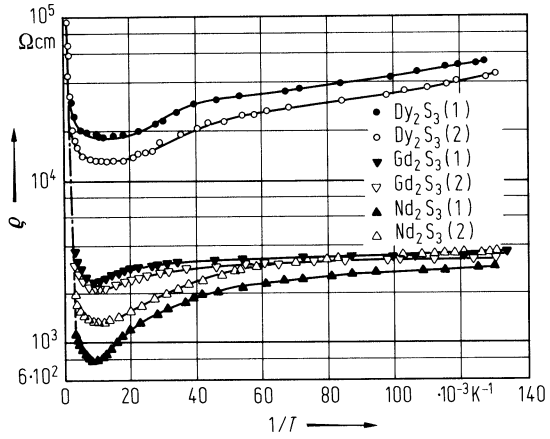

Fig. 12.

γ-Nd_2S_3, γ-Gd_2S_3, γ-Dy_2S_3. Thermoelectric power vs. temperature. The sample compositions are given in Fig. 5 [77T].

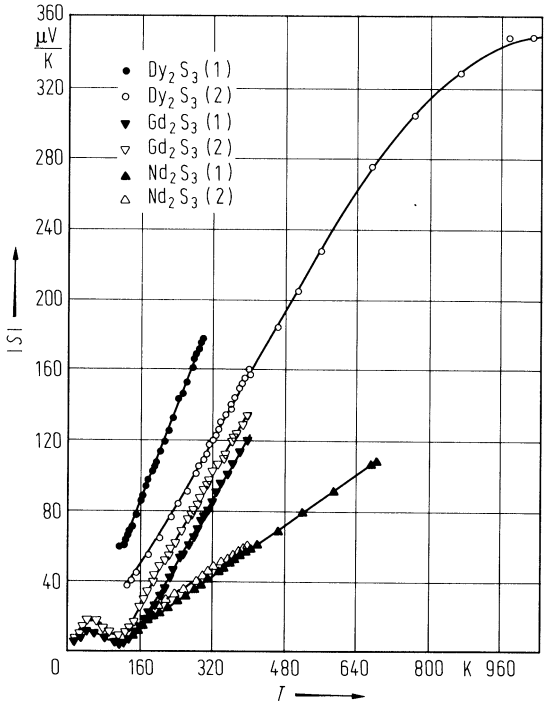

Fig. 13.

γ-Nd_2S_3, γ-Gd_2S_3. Absolute value of the Hall coefficient vs. temperature. The excess metal content is as follows: Nd_2S_3 (*1*): 0.7% Nd, Nd_2S_3 (*2*): 0.65% Nd, Gd_2S_3 (*1*): 0.6% Gd, Gd_2S_3 (*2*): 0.6% Gd [74T].

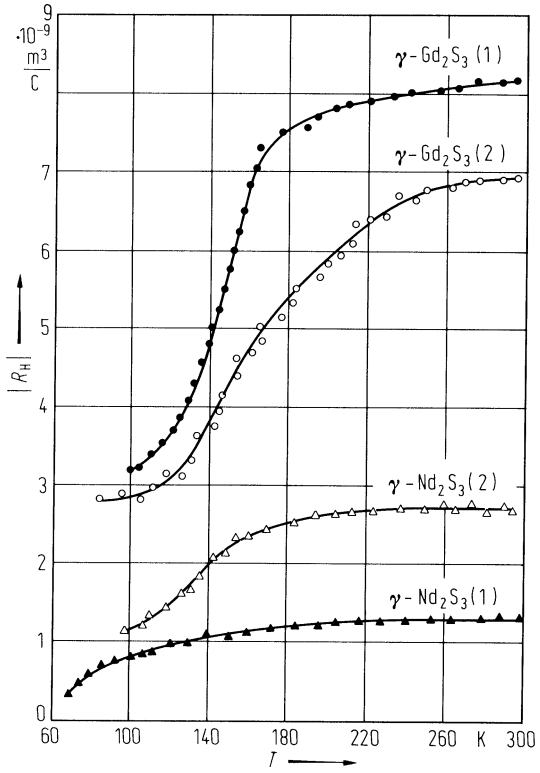

Fig. 14.

γ-Ln_2S_3. MgK_α X-ray photoelectron spectra of the rare-earth sesquisulfides (Ln = La, Ce, Nd, Sm, Gd, Dy) in the energy region below Fermi level down to Ln 5s core level [91K].

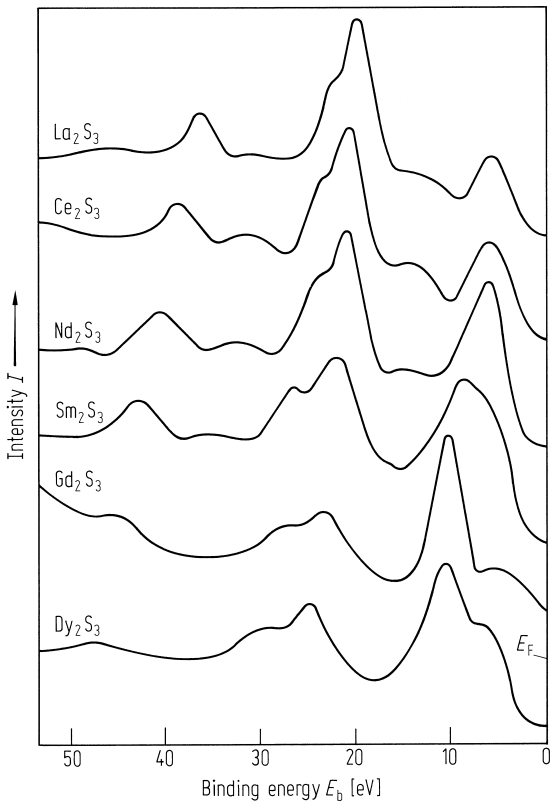

Fig. 15.

γ-Ln_2S_3. MgK_α X-ray photoelectron spectra of the rare-earth sesquisulfides (Ln = La, Ce, Nd, Sm, Gd, Dy) in the 4d core level region [91K]. E_b relative to E_F.

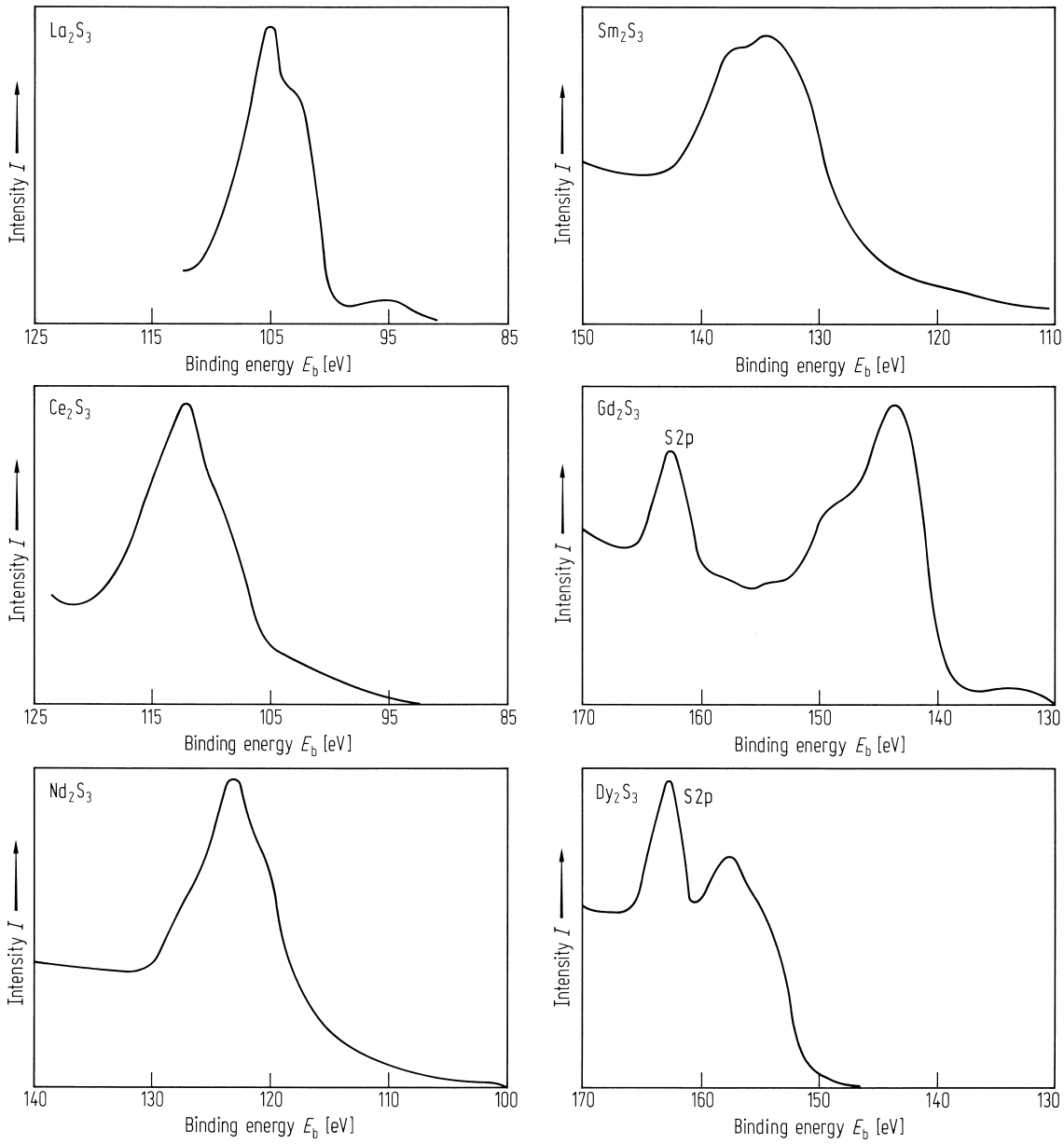

Fig. 16.

γ-Ln_2S_3. AlK_α X-ray photoelectron spectra of the rare-earth sesquisulfides (Ln = La, Nd, Sm, Gd) in the 3d core level region [91K]. The trivalence of Sm is testified by the value of the Sm 3d doublet line spin-orbit splitting (= 27.6 eV). E_b relative to E_F.

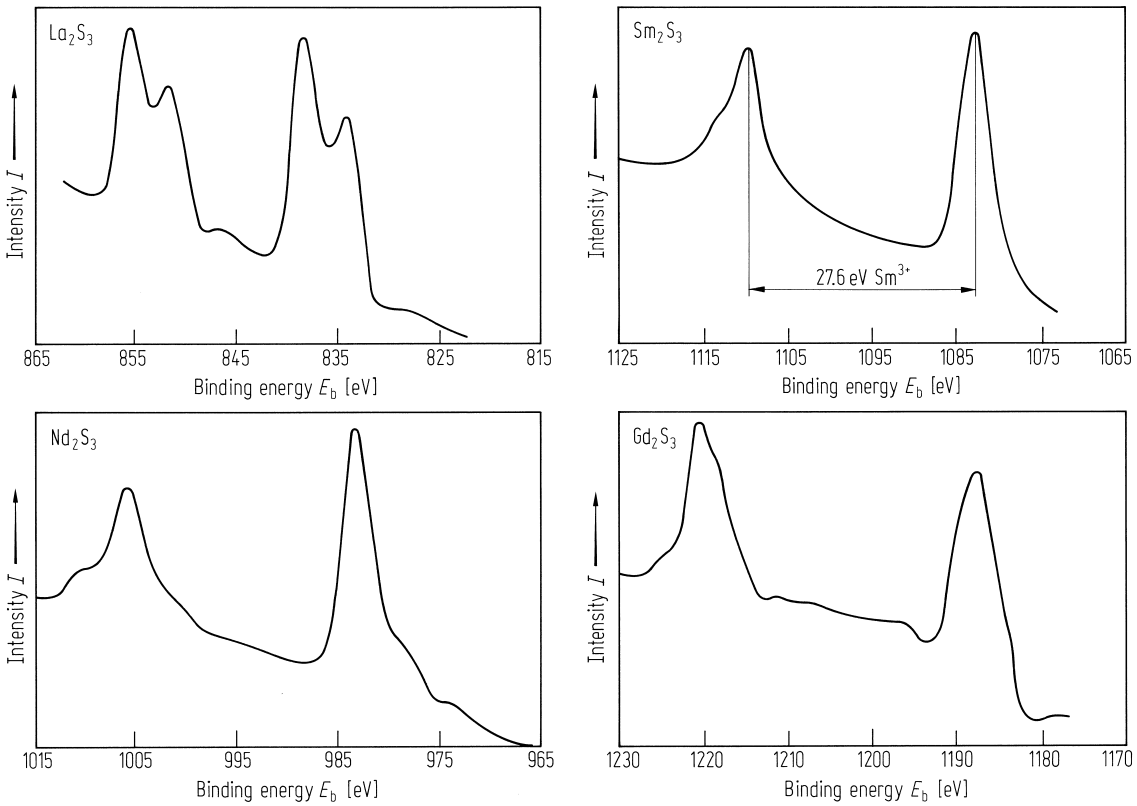

Fig. 17.

γ-Ln_2S_3. Electron loss spectra of the rare-earth sesquisulfides (Ln = La, Ce, Nd, Sm, Gd, Dy) for primary electron beam energy E_p = 750 eV. All the peaks, revealed from the second derivative d^2N/dE^2 are indicated by arrows [91K].

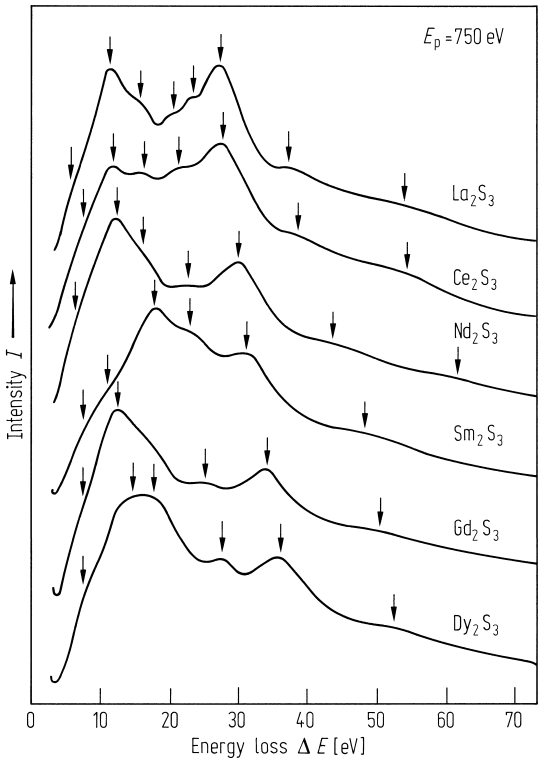

Fig. 18.

γ-Ln_2S_3, Ln = La, Nd, Gd. 4f-4f giant resonance in energy loss spectra at primary electron energy E_p = 750 eV after Shirley background subtraction [91K].